Mechanistic Studies of Surface Polymerization by Ion-Assisted Deposition

ARTICLE *in* THE JOURNAL OF PHYSICAL CHEMISTRY C · FEBRUARY 2007

Impact Factor: 4.77 · DOI: 10.1021/jp067266y

Mechanistic Studies of Surface Polymerization by Ion-Assisted Deposition

Wen-Dung Hsu,[†] Sanja Tepavcevic,[‡] Luke Hanley,*[,‡] and Susan B. Sinnott*[,†]

Department of Material Science and Engineering, University of Florida, Gainesville, Florida 32611-6400, and Department of Chemistry, University of Illinois at Chicago, Chicago, Illinois 60607-7061

Received: November 3, 2006; In Final Form: January 15, 2007

Polythiophene is a conductive polymer that has attracted much interest in recent years because its properties are desirable for applications that include light-emitting diodes, field-effect transistors, and photovoltaics. Optimization of the performance of polythiophene in these devices requires the development of processing methods that can simultaneously control its chemistry and morphology on the nanometer scale. One such method is surface polymerization by ion-assisted deposition (SPIAD) in which conducting polymer thin films are grown on substrates by the simultaneous deposition of hyperthermal polyatomic ions and thermal neutrals in vacuum. Here, mass-selected beams of thiophene ions are deposited on α-terthiophene oligomers in experiments, and density functional theory−molecular dynamics (DFT−MD) simulations are carried out to determine the dominant mechanisms responsible for the SPIAD process. Both neutral and positively charged systems are considered in the simulations in order to assess the effect of charge on the results. The experimental results show that polymerization occurs preferentially under a narrow set of ion energy and ion/neutral ratio conditions. The DFT−MD simulations illustrate the manner in which ion energies affect polymerization and reveal how secondary chemical reactions can substantially modify both the thin film and the substrate.

I. Introduction

Polymers such as polythiophene have generated considerable interest in recent years because of their combination of electrical conductivity, low cost, low weight, and high processability. This combination of properties has led to a wide range of applications in electronic and optical devices including light-emitting diodes, field-effect transistors, photovoltaics, sensor films, recording materials, and rechargeable batteries.[1,2] To optimize the performance of these devices, it is necessary to develop processing methods that can control thin-film chemistry and morphology on the nanoscale.[3,4] One method that has been developed to achieve this result is surface polymerization by ion-assisted deposition (SPIAD) in which conducting polymer thin films are grown on substrates by the simultaneous deposition of hyperthermal polyatomic ions and thermal neutrals in vacuum.[5−10] In this study, the deposition of mass-selected beams of thiophene ions on thin films of α-terthiophene (3T) oligomers on a silicon substrate are carried out in experiments and density functional theory−molecular dynamics (DFT−MD) simulations to determine the dominant mechanisms responsible for the SPIAD process and assess their relative importance. Both neutral and positively charged systems are considered in the simulations in order to quantify the effect of charge on the results.

SPIAD has been performed with both mass-selected ions for mechanistic studies and non-mass-selected ions from a broad-beam ion source for prototyping manufacturing processes. SPIAD can be applied in a combinatorial fashion in that ion energy, ion structure, ion kinetic energy, neutral structure, ion/neutral ratio, and substrate temperature can all be systematically varied to create libraries of candidate films.[11] These film libraries can then be rapidly probed for optimal morphology, film thickness, electronic structure, and target properties.[7,8,12] SPIAD allows fine-tuning of film optical band gaps and other opto-electronic properties by modification of the films' chemical and morphological structure. For example, polythiophene and polyphenyl SPIAD films display narrower band gaps and reduced barriers to hole injection compared with their evaporated film counterparts.[6,9]

SPIAD displays other advantages for the deposition of conducting polymer films, including the absence of entrained solvent molecules and the utilization of sustainable (green) production strategies. However, the greatest advantage of SPIAD lies in its readily available combinatorial capability, which can only be fully utilized by an understanding of the relationship between deposition conditions and film properties. Previous experimental work on SPIAD investigated mechanisms of the ion-induced surface polymerization reactions and determined that polymerization occurs for specific ion/neutral ratios and ion energies.[7,8] Surface polymerization was also shown to form a distribution of species, not just a single oligomer.[6,8] Contrasting experiments with atomic versus polyatomic ions showed that the latter behave as both catalysts and reagents by energetically inducing polymerization and forming adducts with the neutral reagent, respectively.[5] Utilization of SPIAD for combinatorial materials preparation would be greatly facilitated by a comprehensive view of how these various mechanisms contribute to the overall film formation event, but such a mechanistic understanding remains elusive.

The experiments described here utilize a mass-selected beam of thiophene ions to remove fragment ions, radicals, and protons (all present in non-mass-selected ion sources) that can contribute to the film growth process and thereby complicate mechanistic studies of the polymerization event. Mass-selected SPIAD experiments are readily modeled by computer simulations that allow detailed elucidation of mechanistic aspects. Therefore, DFT−MD simulations are also applied to examine energetic

* Corresponding authors. E-mail: lhanley@uic.edu; ssinn@mse.ufl.edu.
[†] University of Florida.
[‡] University of Illinois at Chicago.

10.1021/jp067266y CCC: $37.00
Published on Web 02/27/2007

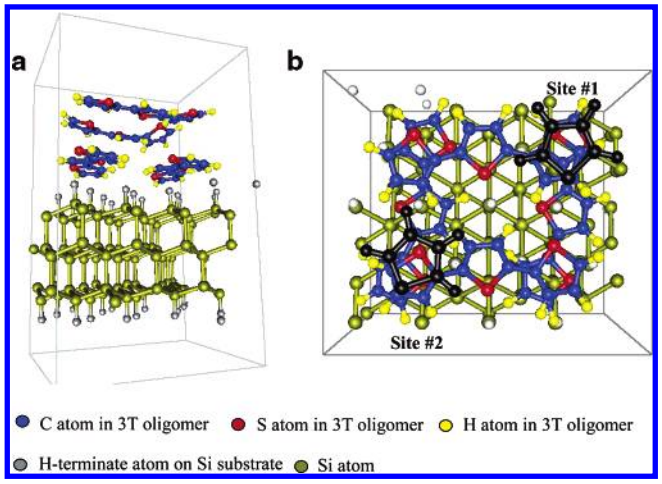

Figure 1. (a) Equilibrium simulation model before deposition. Two layers of 3T oligomers sit on the hydrogen-terminated Si (111) substrate surface. (b) The top view of equilibrium simulation model. Two thiophene molecules marked in black represent the two deposition sites in the simulations.

thiophene molecular deposition on 3T thiophene oligomers. These simulations provide key insight into the complex, cross-link-forming chemical reactions that occur during SPIAD. Comparison of experiments and computer simulations is a powerful strategy in understanding ion-induced surface processes.[13−16]

II. Computational Details

The DFT−MD simulations described here are performed using the CASTEP software[17,18] with the generalized gradient approximation (GGA-PW91). The core electrons are represented by ultrasoft pseudopotentials, and the valence electrons are described with plane waves that have a kinetic energy cutoff of 240 eV, and the *k*-point meshes used in the calculation are $1 \times 1 \times 2$. The convergence of total energy was tested with respect to kinetic energy cutoffs up to 310 eV and *k*-point meshes up to $1 \times 2 \times 2$. The results show that the difference in total energy between the conditions used in the study and the more computationally intensive conditions is within 0.08 eV/atom. This indicates that the conditions used in the DFT−MD simulations represent a good balance between computational efficiency and accuracy.

The simulation system consists of a supercell that is $13.3 \times 15.4 \times 25$ Å^3 and contains three layers of hydrogen-terminated Si (111) covered on one side by a 3T thin film that consists of four 3T oligomers, two of which are arranged parallel to one another and 3.2 Å from the Si surface, while the other two oligomers are arranged parallel to each other but such that the axis drawn through their carbon backbones is perpendicular to that of the first two oligomers. The total number of atoms in the film and substrate is 220 atoms, and the setup is shown in Figure 1a. The distance between the oligomers in the film is about 3.2 Å. The system is allowed to equilibrate for 200 fs prior to thiophene molecule deposition, and the simulations evolve for about 240 fs/collision event. The NVT ensemble is used in all of the simulations to maintain the system temperature at 300 K, and the simulation time step is 1 fs. This system configuration mimics the experimental system in which the oligomers are physisorbed on the silicon surface in random arrangements while at the same time maximizing the contact area in the relatively small supercell necessitated by the high computational cost associated with the DFT−MD simulations. Importantly, the simulations should be able to model localized chemical reactions that occur when ions or neutral molecules collide with the oligomers at locations close to the substrate surface.

The thiophene incident energies considered in the simulations are 100, 200, 250, and 500 eV/molecule. In the case of the three lowest deposition energies, the effect of charge on the deposition process is investigated. In particular, both systems that have a +1 charge and that are neutral are considered. The DFT approach smears the charge throughout the system rather than localizing it on the incident molecules. However, because the simulations represent only a localized portion of the actual experimental system over short (nanosecond) time scales, the comparison of neutral and charged systems is still indicative of what occurs in parts of the experimental system, especially as the incident molecules approach the surface and are increasingly likely to share charge with it. The simulations consider the deposition of a single thiophene particle at each incident energy, except for the 250 eV/molecule deposition case, where two thiophene particles are deposited to investigate the effects associated with higher fluences.

In all of the simulations, the molecules or ions are deposited at the points where the 3T oligomers cross each other (see Figure 1b) to maximize opportunities for cross-link formation. This choice ensures that the most energetic phenomena in the SPIAD process will be investigated in the simulations and shed light on the most complex aspects of polymerization. Because there are four crossed sites in the model and each of them is slightly different in 3T oligomer orientation (the thiophene rings tilt to slightly different degrees and in different directions), in some cases the thiophene molecule or ion is deposited on site no. 1 in Figure 1b, whereas in other cases it is deposited on site no. 2 in Figure 1b. Specifically, site no. 1 is chosen in the 100 eV deposition case and in the first deposition event at 250 eV for the neutral system, whereas site no. 2 is chosen in the 200 eV deposition case, the first deposition event at 250 eV in the case of charged-system, the second deposition event at 250 eV for the neutral system, and at 500 eV. The chemical reactions that occur on deposition are then documented and analyzed.

III. Experimental Methods

SPIAD is performed by combining deposition of thiophene ions with simultaneous dosing of 3T vapor under vacuum. The vacuum apparatus used to perform SPIAD and X-ray photoelectron spectra (XPS) analysis is only briefly described here.[8,19] The apparatus consists of a differentially pumped ion source, a preparation chamber, and an analysis chamber. Thiophene (99+%, Aldrich Chemical Co.) was used as the ion precursor. For the isotopic experiment, we used deuterated thiophene (D_4, 97%, Chambridge Isotope Laboratories Inc). Mass-selected beams of $C_4H_4S^+$ (thiophene) ions are produced by electron impact. Terthiophene crystals (2,2′:5,2″-terthiophene, 99%, Aldrich Chemical Co.) are used as received. Terthiophene dosing is accomplished with a resistively heated homemade source mounted on the preparation chamber whose beam is incident on the surface during ion bombardment. Different ion/neutral ratios are utilized for ion energies in the range of 50−200 eV by changing the fluence of neutrals ($1-6 \times 10^{17}$neutrals/cm^2) or ions ($2-4 \times 10^{15}$ ions/cm^2). Silicon wafers are used as substrates for deposition, after etching with 5% HF to produce the hydrogen-terminated surface H−Si (100) with a minimum of oxide. The HF-etched Si surfaces prior to deposition display an elemental content of 10% C, 4% O, and 86% Si, as recorded by monochromatic XPS. All XPS of the clean substrates and SPIAD films are recorded at 44 eV pass energy and normal

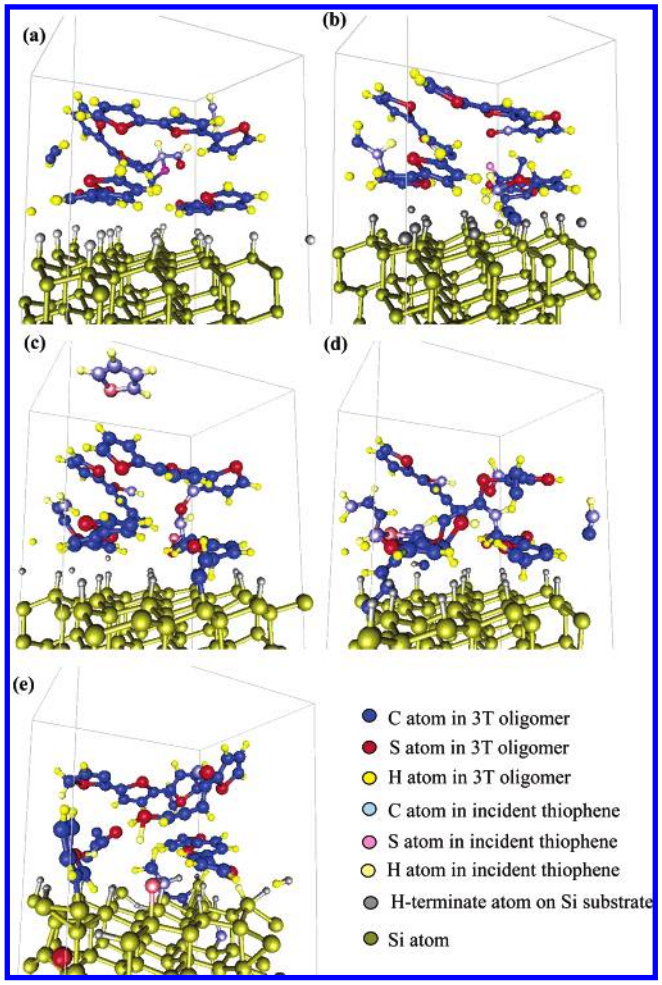

Figure 2. Snapshots from the DFT−MD simulations of the neutral system, which simulate the deposition of a thiophene molecule on a terthiophene oligomer thin film and Si substrate. (a) The final snapshot of deposition in the 100 eV deposition event (time = 240 fs). (b) The final snapshot of deposition in the 200 eV deposition event (time = 240 fs). (c) The final snapshot of the first deposition in the 250 eV deposition event (time = 240 fs). (d) The final snapshot of the second deposition in the 250 eV deposition event (time = 480 fs). (e) The final snapshot of deposition in the 500 eV deposition event (time = 240 fs).

takeoff angle without air exposure following deposition, as described previously.[8,19] SPIAD films are also deposited onto a photopatterned silicon wafer on which a nanostructured oxide layer has been formed (Mass Consortium Corp.) for desorption ionization with 337 nm nitrogen laser radiation followed by mass spectral analysis in a reflectron time-of-flight instrument (Voyager-DE PRO 6275, Applied Biosystems).[6]

IV. Simulation Results

A. Neutral Systems. Figure 2 shows snapshots from the five deposition events considered in the DFT−MD simulations of the neutral systems, where the incident energy ranges from 100 to 500 eV. The molecular weight distribution of the chemical products that are generated after these deposition events are shown in Figure 3. As expected, the higher the deposition energy, the greater the damage to both the incident molecule and the 3T oligomer thin film. In the 100 eV deposition event, shown in Figure 2a, the incident thiophene molecule breaks into two small fragments (C_2H_2 and C_2H_2S) during impact, which chemically modifies only the impacted 3T oligomer. The resulting chemical products (illustrated in Figure 3a) are formed

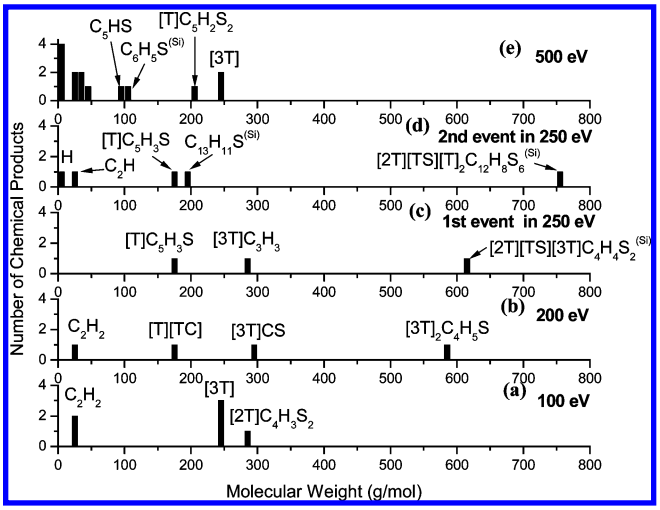

Figure 3. Molecular weight distribution of chemical products that are generated after the neutral deposition events. Chemical products that form bonds with the Si substrate are marked with a (Si) superscript. [TC] and [TS] indicate that there is a C and S atom, respectively, being included in a thiophene ring.

through bonding between these fragments and collision-induced decomposition of the impacted 3T oligomer to form a product such as $[2T]C_4H_3S_2$. There are also two C_2H_2 fragments that form, one from the incident thiophene and the other from the impacted 3T oligomer.

In the 200 eV deposition event, illustrated in Figure 2b, however, the incident molecule breaks into five small fragments (2CH, CH_2, C, S) during impact, breaks apart a thiophene ring within the first layer of the 3T oligomer thin film, and modifies the oligomer chains in the film's second layer. Polymerization occurs between two 3T oligomers in the bottom layer through interactions with the collision fragment C_3H_3, which is generated from an incident thiophene fragment (CH) and an impacted 3T oligomer fragment (C_2H_2). The 3T oligomer, which is adjacent to the impacted 3T oligomer, also undergoes chemical modification, where one H atom is replaced by CS, where the C atom is from the incident molecule and the S atom is knocked loose from the impacted thiophene ring. Other chemical products, such as [T][TC][20] and C_2H_2, are formed as a result of bonding between fragments from incident molecules and fragments from the collision-induced decomposition of the 3T oligomer (see Figure 3b).

The first 250 eV event is somewhat similar to the 200 eV deposition event in that the simulation predicts that the impacting thiophene molecule breaks into six small fragments of three CH, C, S, and H on impact and breaks the impacted thiophene ring of the 3T oligomer (see Figure 2c). The incident energy is high enough that the fragments generated by the impact scatter and modify the oligomers beside and beneath the oligomer at which the initial collision occurs. Consequently, polymerization is predicted to occur through bonding between the oligomers beside and beneath the impact site through a (CH)S(CH) fragment, in which the CH are from the incident molecule and the S is from the impacted thiophene ring. The polymerized chemical product, $[2T][TS][3T]C_4H_4S_2$, is also found to form bonds with the Si substrate. Other chemical products, $[3T]C_3H_3$ and $[T]C_5H_3S$, are formed by adding 3T oligomer fragments and incident molecule fragments. Overall, there are two intact 3T oligomers that remain unchanged following deposition. The majority of the chemical products produced are trapped between the top and bottom 3T oligomer layers. The molecular weight distribution of these products is summarized in Figure 3c.

TABLE 1: Statistical Analysis of Deposition Results Predicted by the Simulations[a]

incident energy	100 eV		200 eV		250 eV			500 eV
deposition event	1(neutral) (site no. 1)	1(charged) (site no. 1)	1(neutral) (site no. 2)	1(charged) (site no. 2)	1(neutral) (site no. 1)	1(charged) (site no. 2)	2(neutral) (site no. 2)	1(neutral) (site no. 2)
total no. of products	6	5	4	5	3	4	4	14
% products bonded to Si substrate	0%	0%	0%	25%	33%	33%	50%	57%
% intact 3T rings	75%	67%	50%	42%	50%	58%	17%	50%
no. surface polymerization reactions	0	0	1	0	1	1	1	0

[a] "Intact" means that the C and S atoms in the thiophene ring maintain the same hybridization as they had initially.

A second 250 eV deposition event is performed on the system modified by this first event that targets a different location on the surface, as shown in Figure 2d. This chemically modifies the targeted oligomer, which polymerized during the course of the first deposition event, and the oligomer beneath it. Thus, over the course of these two deposition events every 3T oligomer on the surface is chemically modified and fragmentized. Some of the chemical products, such as [2T][TS]-$[T]_2C_{12}H_8S_6$ and $C_{13}H_{11}S$, evolve from the products formed in the first collision event, whereas others, such as C_2H and H, are formed from the bonding of small incident molecule fragments and 3T oligomer fragments. Because of the large extent of modifications of the 3T oligomers in the film following these two deposition events, simple surface polymerization between two 3T oligomers is no longer present. Instead, large fragments bond to one another to create a new chemical product, such as $[2T][TS][T]_2C_{12}H_8S_6$, with a larger overall molecular weight. Again, most of the energetic fragments that are produced are ultimately trapped between the top and bottom oligomer layers. A detailed summary of the chemical products that are formed after the second deposition event is given in Figure 3d.

In the 500 eV deposition event, illustrated in Figure 2e, the incident thiophene molecule breaks into individual atoms or CH fragments when it collides with the surface. The impacted thiophene ring is also broken into individual atoms of 3C, 3H, and S. These products and incident molecule fragments then collide with the bottom layer of oligomers and break them apart because of their high kinetic energy. Additionally, some of the fragments form chemical bonds with the Si substrate by the end of the simulation. In other words, a small collision cascade is predicted to occur and most of the energetic fragments that are produced are trapped between the Si surface and the bottom layer of the 3T oligomer thin film or form covalent bonds to the Si substrate. The chemical products are much smaller than the products produced at the lower incident energies, as shown in Figure 3e, and there are only two 3T oligomers that remain intact after the deposition process is complete.

Table 1 provides a statistical analysis of the chemical products predicted from the simulations. As expected, the total number of chemical products varies substantially with deposition energy. In addition, the percentage of chemical products that are covalently bonded to the underlying Si substrate increases as the deposition energy increases. The percentage of intact 3T oligomer thiophene rings also decreases as the deposition energy increases until 250 eV, after which this percentage remains essentially unchanged. Furthermore, increasing the number of deposited thiophene molecules further decreases the percentage of intact 3T oligomer thiophene rings. Last, surface polymerization between 3T oligomers is predicted to occur at incident energies of 200 and 250 eV.

B. Charged Systems. Table 1 also lists the results of statistical analysis of the chemical products that are produced in the charged systems. It indicates that the differences in the collision outcomes between the neutral events and the positively charged events are small in most cases. However, a careful comparison of the forces and velocity variations of the atoms in the system (data not shown) indicate that the atoms in the +1 charged system experience slightly larger forces and velocity variations than the atoms in the neutral system. The results further indicate that the system with the +1 charge makes the potential well between the atoms slightly deeper than that in the case of the neutral system.

In the case of the 100 eV deposition event, the results and mechanisms for the neutral and charged systems are very similar. The deposited thiophene ion breaks into C_3H_3 and CHS fragments during the initial collision. The incident energy is only sufficient enough to modify the impacted 3T oligomer. Thus, there are two intact 3T oligomers that remain following deposition and one 3T oligomer that is beneath the impacted 3T oligomer and has been slightly modified through the adsorption of a S atom from the impacted thiophene ring. Other chemical products include a large fragment from the collision induced decomposition of a 3T oligomer, such as $[2T]C_2H$, and a ring-shaped molecule (C_6H_6S) formed from bonding of the incident thiophene fragments (C_4H_4S) and a fragment of an impacted 3T oligomer (C_2H_2). A snapshot of the system following deposition is shown in Figure 4a, and the chemical products are summarized in Figure 5a.

In the case of 200 eV deposition, illustrated in Figure 4b, the incident ion breaks into four fragments, 3CH and CHS, during impact. The 3T oligomer that had a H atom be replaced by a CS fragment in the neutral case now remains intact. Other chemical products, $[3T]C_3H_2S$ and $[3T]C_3H_4$, are formed from bonding between the incident molecule fragments and 3T oligomers. Chemical products, such as [T][TC][20] and CS, are formed from bonding of 3T oligomer fragments and thiophene ion fragments (see Figure 5b). There are two major differences between the neutral and charged cases. The first is that there is a chemical product, $[3T]C_3H_2S$, that forms a bond with the Si substrate in the charged case. In the neutral case, the same fragment, C_2H, from the impacted thiophene ring that forms the $[3T]C_3H_2S$ bond to the Si substrate is instead bonded to a H-terminated atom from the Si substrate to produce HCCH. The second is that there is no surface polymerization observed in the charged case but there is in the neutral case. Additionally, in the case of the charged system, the fragment that contributes to surface polymerization in the neutral system instead bonds to a hydrogen atom that is knocked out of the incident thiophene molecule. This prevents the fragment from forming a bond to another 3T oligomer to polymerize the film. These differences illustrate how scattered hydrogen atoms can restrain surface polymerization even when the deposition energy is high enough to trigger the process.

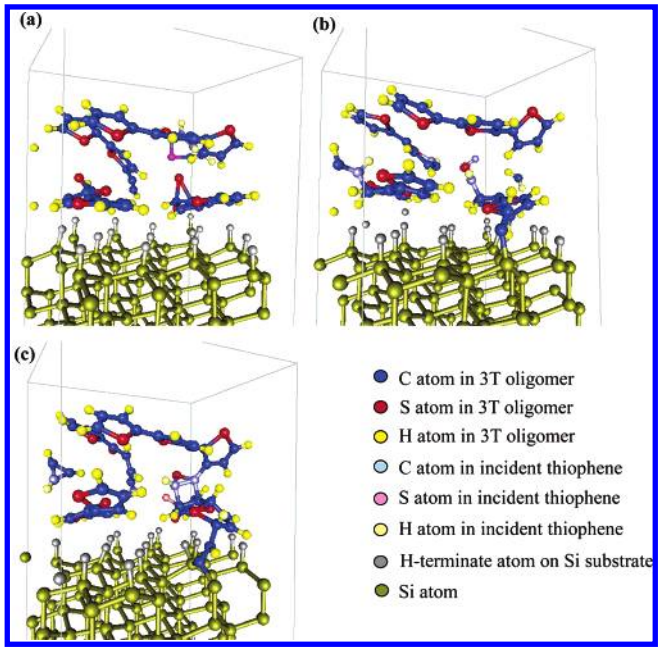

Figure 4. Snapshots from the DFT−MD simulations of the +1 charged system, which simulate the deposition of a thiophene molecule on a thiophene thin film and Si substrate. (a) The final snapshot of deposition in the 100 eV deposition event (time = 240 fs). (b) The final snapshot of deposition in the 200 eV deposition event (time = 240 fs). (c) The final snapshot of the deposition in the 250 eV deposition event (time = 240 fs).

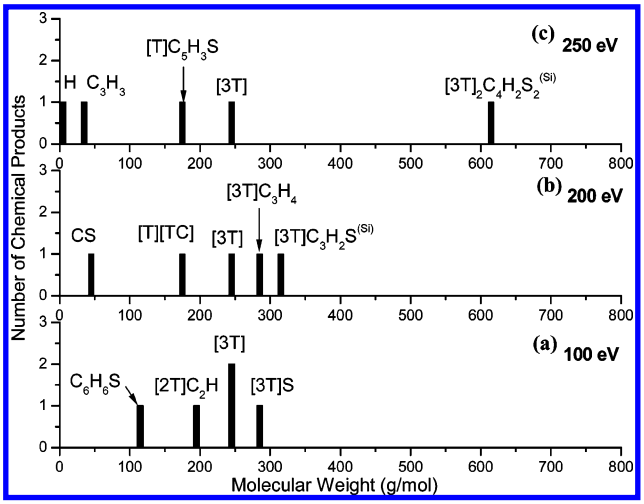

Figure 5. Molecular weight distribution of chemical products that are generated after the positively charged deposition events. Chemical products that form bonds with the Si substrate are marked with a (Si) superscript. [TC] and [TS] indicate that there is a C and S atom, respectively, being included in a thiophene ring.

In the case of the 250 eV deposition event (Figure 4c), the incident thiophene ion breaks into six small fragments (three CH, C, S, and H) on impact and breaks a thiophene ring on the targeted 3T oligomer. Although the target site is different from the target site in the neutral case (the impacted thiophene ring tilts around 30° toward to Si substrate in this case, while the impacted thiophene ring tilts only about 10° toward to Si substrate in the neutral case), the same polymerization mechanism is predicted to occur in both cases. In particular, polymerization occurs through bonding of the oligomers next to and beneath the impacted oligomer by CS(CH) fragments, where C and CH are from the incident molecule or ion and S is from the impacted thiophene ring. This result indicates that the DFT−MD simulations are able to capture the key mechanisms that contribute to the complicated surface polymerization phenomenon in ion-assisted deposition. Other chemical products ([T]C_5H_3S and C_3H_3) are formed by adding 3T oligomer fragments and incident ion fragments, and the results are shown in Figure 5c. It is also predicted that some of the products are covalently bonded to the underlying Si substrate and, overall, there are two intact 3T oligomers that remain unmodified following deposition.

C. Hybridization Analysis. Examination of the change in the number of sp^2-hybridized carbon atoms is another way to characterize the extent of system chemical modification as a result of deposition. Prior to deposition, all of the carbon atoms in the 3T oligomers and incident thiophene molecule are sp^2-hybridized. When the incident thiophene impacts the 3T oligomer, the hybridization of the carbon atoms change if they are involved in chemical reactions. Transition-state carbon atoms, with temporarily more than four neighbors, are also monitored. Similar transition-state hydrogen and sulfur atoms are also observed in the simulations. The percentages of transition-state carbon atoms that are generated immediately following the thiophene molecule collision range from 4% in the cases of 100 eV/molecule collisions to 17% in the case of the 500 eV/molecule collision. Following the initial collision, the transition-state atoms move away from the impact side and modify the 3T oligomers, simultaneously transforming to more stable hybridization states. Most of the transition-state atoms finish reacting within 30 fs of each collision. In addition, a small number (<4%) of new transition-state atoms is generated during the equilibration process as part of additional atomic rearrangements. Importantly, all of the transition-state atoms have completely reacted by the end of the equilibration process that follows deposition and are ultimately part of the chemical products discussed above.

Table 2 provides details of the hybridization states and transition states of carbon atoms in the simulations. The number of transition-state atoms is summed from each MD step. The hybridization states are obtained from the final equilibration. It is found that the sum of the transition-state atoms increases as the deposition energy increases but decreases at the highest 500 eV incident energy. This is because in the 500 eV deposition event the incident energy is high enough for the fragments to scatter over a large fraction of the supercell and to penetrate into the Si substrate. Thus, the incident energy dissipates more efficiently, which restrains the transition-state atoms from regenerating during equilibration. In the case of the 200 and 250 eV deposition events, the fragments are generally trapped between the upper-layer 3T oligomers and bottom-layer 3T oligomers. Thus, although the transition-state atoms are fewer than in the 500 eV deposition event immediately following impact, more transition-state atoms on the whole are formed at 200 and 250 eV. The number of transition-state carbon atoms is slightly smaller in the neutral case than in the charged case for 100 and 200 eV, while the opposite is true for 250 eV.

In general, after deposition the amount of sp^2 hybridization decreases as the deposition energy increases, which indicates the greater degree of modification of the 3T oligomers at higher energies. Comparing the neutral and charged system results, Table 2 indicates that the charged systems have less sp hybridization than the neutral systems. In other words, carbon atoms in charged systems generally have more neighboring atoms than neutral systems after equilibration is complete. The result is consistent with the finding that the potential well

TABLE 2: Chemical State of the Surface Carbon Atoms Following Each Deposition Event

incident energy	100 eV		200 eV		250 eV			500 eV
deposition event	1(neutral) (site no. 1)	1(charged) (site no. 1)	1(neutral) (site no. 2)	1(charged) (site no. 2)	1(neutral) (site no. 1)	1(charged) (site no. 2)	2(neutral) (site no. 2)	1(neutral) (site no. 2)
sum of transition-state atoms	34	52	117	127	174	164	182	99
sp hybridization	7.69%	3.85%	7.69%	1.92%	5.77%	3.85%	12.50%	19.23%
sp^2 hybridization	90.38%	94.23%	82.69%	88.46%	90.38%	84.62%	69.64%	75.00%
sp^3 hybridization	1.92%	1.92%	9.62%	7.69%	3.85%	11.54%	16.07%	5.77%
terminal C atom	0.00%	0.00%	0.00%	1.92%	0.00%	0.00%	1.77%	0.00%

between the atoms in the charged-system is slightly deeper than that in the neutral system. Thus, carbon atoms more readily attract and bond to neighboring atoms in charged systems, which results in higher degrees of hybridization.

IV. Experimental Results

In conjunction with these simulations, experimental SPIAD is performed by combining the deposition of thiophene ions with the simultaneous dosing of 3T vapor. The vacuum apparatus and conditions used to perform SPIAD and XPS analysis are similar to those used in previous studies.[8,19] The incident ion energy and the ion/neutral ratio are correlated parameters for efficient ion-induced surface polymerization. Therefore, experiments are performed in which the ion energy is varied from 25 to 200 eV and the ion/neutral ratio is varied from 1/50 to 1/900. The extent of polymerization is determined from XPS by measuring the S/Si ratio, which increases as an organic film is formed on the Si substrate from the thiophenic species.

By varying the ion/neutral ratio at a constant ion energy of 200 eV, it is determined that polymerization occurs in a well-defined region of ion energy and ion/neutral ratio space. Figure 6 compares the S/Si ratio from XPS for direct ion deposition at various fluences (empty bars, no 3T dosing) with SPIAD at similar ion fluences ($\sim 10^{15}$ ions/cm^2) at various ion/neutral ratios (solid bars). Figure 6a shows that polymerization occurs at 200 eV for ion/neutral ratios of 1/150, 1/450, and 1/900 but not for 1/50. For 200 eV deposition, an ion/neutral ratio of 1/150 is optimal because it shows the largest ($\sim 10\times$) increase in S/Si ratio compared to direct ion deposition at similar ion fluence. In contrast, the 1/50 ratio shows a decrease in S/Si ratio compared to direct ion deposition (Figure 6a).[8,19]

Varying both the ion energy and the ion/neutral ratio indicates that lower ion/neutral ratios are optimal for polymerization at lower ion energies. Figure 6 illustrates that the optimal ion/neutral ratios are 1/100 for ion energies of 100 eV, 1/75 for 50 eV, and 1/50 for 25 eV. This is likely due to the reduced ion-induced desorption of 3T oligomers at lower ion energies, which requires less 3T deposition.[10] All SPIAD films are stable in vacuum for over 4 h, a period during which pure 3T films are observed to completely sublime. The C/S ratio is around four for all SPIAD and direct ion deposited films (data not shown), which is consistent with thiophene-containing species.

The mass spectra (MS) of the SPIAD films are shown in Figure 7 and are obtained by laser desorption from films directly deposited onto nanoporous silicon oxide substrates. Previous work used isotopic distributions to assign the observed mass spectra.[6] The ion/neutral ratio used for MS experiments of each ion energy shown is the optimal value determined by XPS, as discussed above. Many smaller polymerization products, such as $[3T]_2^+$, are observed by MS for all ion energies from 25 to 200 eV. However, the 50 eV SPIAD film displays the highest molecular weight species, with peaks as large as $[3T]_4^+$ (see

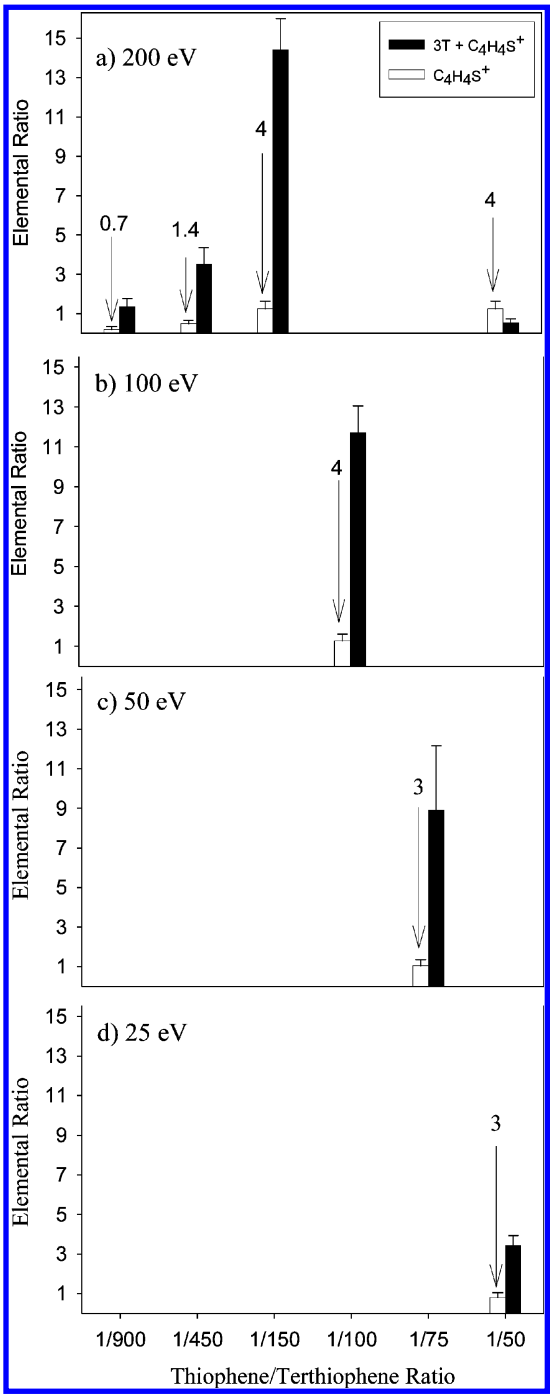

Figure 6. S/Si elemental ratio from XPS for direct ion deposition at various fluences (empty bars) compared with S/Si ratios for SPIAD at similar ion fluences ($\sim 10^{15}$ ions/cm^2) for various ion/neutral ratios (solid bars). The numbers on the arrows for the direct deposited films correspond to actual ion fluences ($\times 10^{15}$ ions/cm^2). Data recorded at the four ion energies shown.

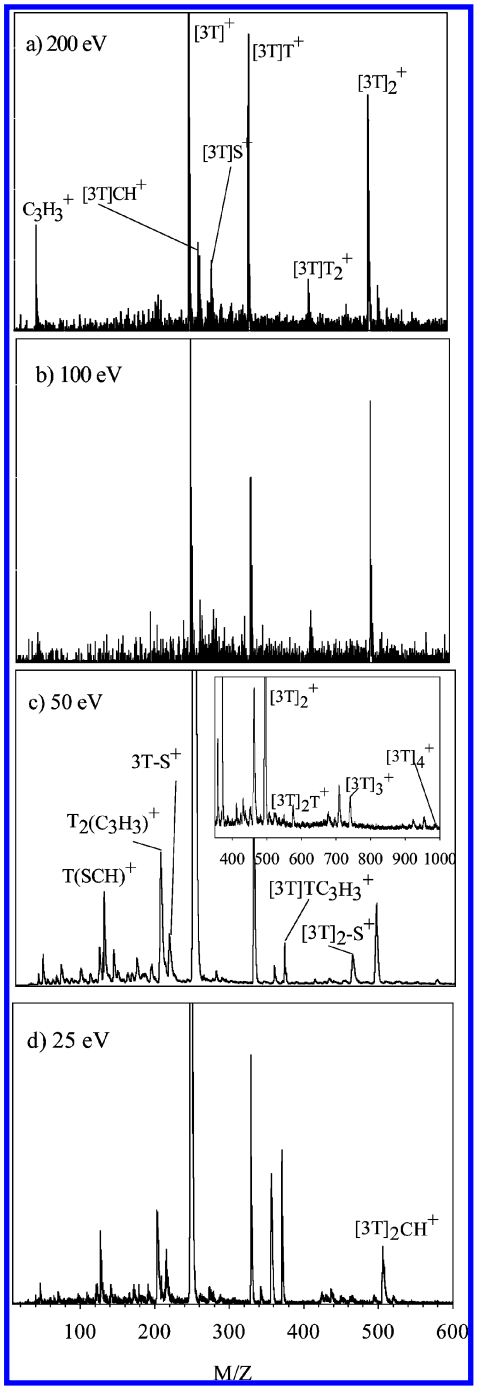

Figure 7. Mass spectra (MS) of the SPIAD films at four ion energies and the optimal ion/neutral ratios (from Figure 5), obtained by laser desorption of conducting polymer films that have been deposited directly onto nanoporous silicon oxide substrates.

the inset in Figure 7c). Formation of the polymerization products $[3T]_x^+$ ($x = 2-4$) are indirectly induced by hyperthermal ion impact. Additionally, a unique series of adduct species displaying loss or pickup of a single sulfur atom are observed. Sulfur atom loss species include $[3T]_x - S^+$ ($x = 1-4$), and sulfur atom pickup species include $[3T]S^+$. In contrast, deposition of only 3T neutrals on the DIOS substrate leads to the appearance of only $3T^+$.[11] Previous results show that most of the ions observed from SPIAD films display a mixture of protonated and radical cations, indicating the presence of free hydrogen in the films.[5]

The mass spectra across 25−200 eV display many similar peaks, but there are other differences besides those noted above

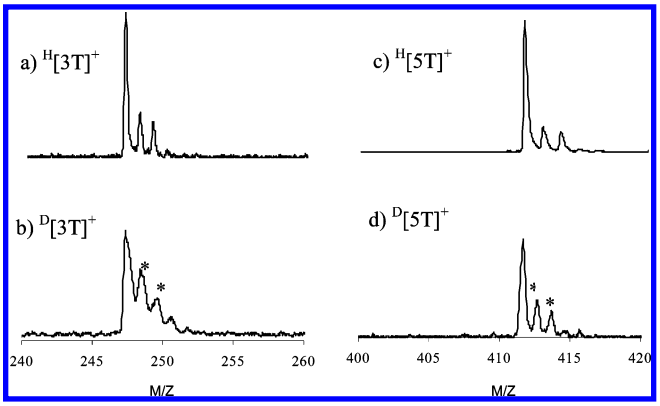

Figure 8. Mass spectra of $^{H}T^+$ and $^{D}T^+$ SPIAD films grown on nanostructured silicon oxide (DIOS) substrate at 50 eV ion energy.

for 50 eV films. SPIAD film mass spectra (100 and 200 eV) are very similar and display peaks up to $[3T]_2^+$, $[3T]T^+$, and other adduct-3T species. Higher mass peaks are observed in these spectra occasionally, including $[3T]_2CH_2^+$, $[3T]_2TC_3H_3^+$, and $[3T]_2T_2CHS^+$ (data not shown). The 25 eV SPIAD film shows the formation of a strong $[3T]_2CH^+$ signal and only a weak $[3T]_2^+$ signal, in addition to the 3T signal.

To further investigate the mechanism of polymerization, SPIAD is performed with deuterated thiophene ions combined with the evaporated 3T neutrals and compared with SPIAD by hydrogenated thiophene ions at otherwise similar conditions. Figure 8 shows mass spectra of the SPIAD films at 50 eV with hydrogenated (a and c) and deuterated (b and d) thiophene ions in the mass ranges of 3T and 5T peaks. Deuterated thiophene ion deposition does not shift the 5T peak at *m*/*z* 411 toward higher masses, indicating that only thiophene fragments are introduced into the film. Large differences can be seen in the intensity of the (M + 1) peaks of $^{D}[5T]^+$ versus $^{H}[5T]^+$, and similar intensity increases are observed for some higher peaks such as 7T (data not shown). $^{D}[5T]^+$ and $^{H}[5T]^+$ show similar values for (M + 2) peaks. The largest deuterated thiophene ion that could have incorporated into the film would be $C_4D_1 - 2S^+$, but this could lead to the formation of (M + 1) and (M + 2) peaks for 5T only if an additional, nondeuterated thiophene monomer is made available by fragmentation of 3T. However, a more likely interpretation of the deuterated ion results is that only small deuterated thiophene fragments are incorporated into the films.

V. Discussion

A. Mechanisms Supported by Experimental Data and Simulations. Several processes occur during deposition that are both detected in the experiments and predicted by the simulations that shed light on the most important bond dissociation and polymerization mechanisms that occur during SPIAD. For example, both simulations and experiments indicate that incident thiophene ions break apart on collision with the 3T film. In particular, $C_3H_3^+$ is seen experimentally at 200 eV and has previously been observed to result from the dissociative scattering of thiophene ions from surfaces in a process referred to as surface-induced dissociation.[16]

Both experiments and simulations indicate that incident thiophene ions undergo dissociation during deposition. Comparing SPIAD deposition of deuterated versus hydrogenated thiophene ions, the mass spectra do not show any shift (Figure 8) expected if there had been incorporation of an intact, deuterated thiophene unit. This is in agreement with the simulation results that predict that intact thiophene ions do not

survive the collisions with the surface. Adducts such as $[3T]T^+$ at 25 eV and $[3T]_2T^+$ at 50 eV that are seen experimentally might be the result of dissociation of 3T neutrals upon ion impact. Previous results with non-mass-selected ion deposition show that most of the ions observed from SPIAD films display a mixture of protonated and radical cations, indicating the presence of free hydrogen in the films.[5] Comparing Ar^+ and T^+ SPIAD films prepared with non-mass-selected Ar^+ and T^+ ions and 3T neutrals it was shown that most of the extra hydrogen originates from incident thiophene ions because Ar^+ SPIAD films did not show a high-intensity M + 1 peak.

Both the experiments and simulations indicate that incident thiophene ions chemically modify the structure of the oligomer film by covalently bonding to 3T oligomers. This covalent bonding occurs primarily via incident thiophene fragments and small 3T fragments to form adducts such as $[3T]C_3H_4^+$, $[3T]C_2H_2^+$, $[3T]_2TS^+$, and $[3T]_2CH^+$ observed in the experiments and [3T]CS, $[3T]C_xH_y$ ($x = 3$, $y = 3,4$), and $[3T]_2C_xH_yS_z$ ($x = 4$, $y = 5,2$, $z = 1,2$) in the simulations. The combination of experiments and simulations provide important information regarding the surface polymerization of 3T oligomers. Thiophene ion fragments are thought to act as polymerization initiators. In the simulations, C atoms that come from the incident molecules or broken 3T rings have high kinetic energy and readily abstract hydrogen atoms from other 3T molecules or directly add on to other 3T molecules. Once this process occurs on two adjacent 3T molecules, it is highly likely that these molecules will bond to each other.

Hyperthermal protons can also trigger the formation of polymerization initiators in a process that is similar to the behavior of hyperthermal organic cations, where the kinematic nature of proton collisions with simple organic molecules condensed on the substrate is exploited to preferentially break C−H bonds.[21] The simulations also show that hydrogen atoms may, however, act as restraining agents to prevent surface polymerization. Because polymerization relies on the bonding of chemical products through carbon atoms, scattered low-energy hydrogen atoms may react with terminating carbon atoms and decrease the probability of cross-link formation between fragments. Importantly, the S atom transfer observed experimentally is also predicted to occur in the simulations.

The experiments and simulations further indicate that fragmentation of the 3T oligomers is an important mechanism in SPIAD. Products such as $[2T]C_4H_3S_2$ in the 100 eV neutral system deposition event, $[2T]C_2H$ in the 100 eV charged system deposition event, [T][TC][20] in the 200 eV neutral and charged system deposition events, $[T]C_5H_3S$ in the first deposition event of the 250 eV neutral and charged systems, $[T]C_5H_2S_2$ in the 500 eV deposition event, and $[2T][TS][T]_2C_{12}H_8S_6$ in the 250 eV second deposition event involve dissociation of a 3T oligomer through direct impact are predicted to occur in the simulations. Similar products, such as $[T]_2C_3H_3^+$ and $[3T]TC_3H_3^+$, are also observed experimentally by MS at 25 and 50 eV. Analogous products seen at 100 and 200 eV correspond to $[3T]_2T_2C_xH_y^+$. In addition, products such as $3T\text{-}S^+$ and $T_2C_3H_3^+$ are observed experimentally at 50 eV and the formation of similar (albeit not identical) species is predicted by the simulations. The fact that similar classes of products form in the simulations and are observed in the experiments highlights the usefulness of this combined computational and experimental approach to studying SPIAD, despite the inherent differences in the systems under consideration.

The simulations also predict that the amount of small fragments (molecular weight <50 g/mol) increases in the 250 eV second deposition event and in the 500 eV deposition event. Examples of these products are S, H_x, where $x < 2$, and C_xH_y, where $x < 2$ and $y < 2$. Some of these products form bonds with the Si substrate and some of them embed into the thiophene thin film. These predictions are supported by experimental data that indicates a drop in polymerization efficiency for higher ion/neutral ratios. It should be pointed out that the experiments require high neutral fluxes because 3T does not permanently stick to surfaces under vacuum due to very low binding energy (see below).

The simulations performed here predict that the incident thiophene molecules damage the structure of the 3T oligomers locally and the incident molecules also break apart on collision with the surface. They further indicate that the C atoms, which come from the incident molecules or broken 3T oligomers, have high kinetic energy. Thus, they are energetic and readily abstract hydrogen atoms from other 3T molecules or adduct on other 3T molecules directly. This is a polymerization initiation process. Once this process occurs on two adjacent 3T oligomers, it is highly likely that these molecules will bond to each other. The simulations therefore predict that in an ideal case where one incident thiophene molecule is in contact with two 3T molecules on its two sides the most efficient energy for surface polymerization should be slightly higher than the C−H bond energy in the thiophene ring. In the experiments, it is difficult to ensure this ideal case. Thus, the incident molecules should generally have enough energy to produce energetic atoms and/or polyatomic fragments that will subsequently react with 3T molecules and initiate the polymerization process. This energy should correspond to the energy required to dissociate a thiophene ring plus the energy that will be dissipated through the film and surface through the collision process.

Similarly, balance is required for the ion/neutral ratio to generate the proper polymerization between 3T oligomers. Too many hyperthermal ions (two vs one) cause a decrease in polymerization efficiency, more fragmentation, and ion-induced desorption. Increasing the energy/molecule results in more damage to and desorption of the 3T oligomers, but it also produces more polymerization initiators. Thus, the amount of energy in the system should be a balance between damaging or desorbing 3T thiophene oligomers and forming new polymerization initiators.

B. Differences Between Simulations and Experiments. There are several fundamental differences between the experiments and simulations that must be taken into account, despite the large area of agreement between the two. Some of these differences are probably not that significant. For example, the effect of the ~1 eV internal energy of the incident ions[16] is relatively small compared to the incident ion energy and probably negligible compared with other differences between the simulations and experiments. Furthermore, ion−molecule reactions following desorption may affect the degree of protonation in the experimental mass spectra, but the general observation of polymerization and adduct formation have been previously supported by ancillary analysis methods.[5,6,8,11] Nevertheless, there are other important differences between the experiments and simulations that must be addressed individually.

The efficiency of energy transfer during deposition is different in the simulation and experimental systems. This can be attributed to several factors. There is a difference in effective surface coverage between the experimental and computational systems: the experimental systems consist of thicker 3T films than are considered in the simulations. The 3T multilayer present experimentally is expected to recoil more than a 3T bilayer upon

thiophene ion impact, as suggested by previous experiments studying the scattering of thiophene ions off of disparate surfaces.[22] Different surface coverage configurations influence the dissipation of incident energy because the softer organic layer recoils more upon hyperthermal ion impact than a stiff semiconductor substrate. In addition, although the SPIAD process uses ions, it is not clear whether or not these ions are neutralized as part of the deposition process and, if they are, it is not clear at what point this would occur along the incoming trajectory. For example, neutralization could occur above the surface or within the film, adjacent to the 3T oligomers. This uncertainty provides additional justification for the simulation of the behavior of both ions and neutrals.

Another significant difference can be attributed to the fact that the deposition sites chosen for the simulation are direct impact sites that need higher incident energies to damage the 3T oligomers. In contrast, the experimental impact sites vary from direct to grazing (i.e., integrated over all possible impact parameters). Thus, the incident ions might experimentally just graze the 3T oligomers and generate only minor damage, which could generate fragments with terminated carbon atoms or transition-state atoms to initiate the surface polymerization process. The incident energy to fulfill this surface polymerization process is much less than the direct impact.

Related to the above differences is that of collision number. The experimental data result from multiple ion−surface collision events combined with continual redosing of the surface with 3T. The simulations involve either one or two collisions per simulation.

The system size is also confined in the simulation compared with the experiment. Thus, the incident energy can only be dissipated within the supercell. This allows the higher incident energy simulations to show greater modification of 3T oligomers than the corresponding experiments. Consequently, direct comparison of incident energies between the simulations and experiment might not be strictly correct. However, the trends predicted in the simulations and observed in the experiments are comparable to one another.

The substrates are also not identical in the computational and experimental systems. The simulations use clean, flat, hydrogen-terminated silicon substrates, whereas the XPS experiments use flat silicon surfaces and the mass spectra use nanostructured silicon oxide covered substrates. However, these substrate differences are less relevant here for several reasons. The phenomena of greatest interest occur between 3T oligomers and incident ions and are therefore largely independent of the nature of the substrate. The chemical reactions predicted in the simulations to occur between the surface and the 3T oligomers or the incident ions cannot be directly observed experimentally by the methods utilized here, as discussed above.

Yet another significant difference between the experimental and computational systems is their time scales. Specifically, the simulations consider phenomena and relaxation events that occur on the order of several picoseconds, whereas the experiments consider phenomena that occur over hours. Thus, the reactive species formed in simulation (i.e., C or H atoms) may take longer than the simulation time scale to form the polymerization products observed experimentally. In addition, the experiments allow rearrangement and reorganization over time.

Last, the experimental conditions are sufficient to stimulate electronic excitation processes that could influence the chemical reactions that occur. In contrast, the DFT−MD simulations do not allow electronic excitations to occur.

Despite all of these differences, the simulations are able to provide important insight into the chemical reactions that occur during deposition, the most significant of which appear to occur on the same time scale as the simulations.

V. Conclusions

The combination of the two strategies vastly improves the mechanistic understanding of the use of SPIAD for the growth of conducting polymer thin films, despite the significant differences between the experiments and simulation. Variation of the experimental reaction conditions indicates that polymerization occurs preferentially under a narrow set of ion energy and ion/neutral ratio conditions. The first-principles MD simulations reported here illustrate the manner in which ion energies affect polymerization and other chemical reactions that modify the substrate. Specifically, ideal incident energies should be balanced between values that are too high and lead to damage or desorption of the α-terthiophene on the substrate, and values that are too low to produce the necessary polymerization initiators. Importantly, this study indicates that polymerization and fragmentation of ions and/or neutral species are critical steps in the SPIAD process. In addition, the simulations predict that free protons and other radicals are formed during SPIAD that could potentially survive for long enough time scales to contribute in a significant manner to the properties of the conducting polymer. This insight can be used to optimize the SPIAD process for polythiophene and other conducting polymer systems. More generally, studies such as this indicate that it should be possible to use computational studies to guide experiments toward the production of optimized films for particular applications.

Acknowledgment. We gratefully acknowledge the support of the National Science Foundation, through grant CHE-0200838 for W.-D.H. and S.B.S. and grant CHE-0241425 for S.T. and L.H.

References and Notes

(1) Fichou, D. *Handbook of Oligo- and Polythiophenes*; Wiley-VCH: Weinheim, Germany, 1999.

(2) Heeger, A. J. *J. Phys. Chem. B* **2001**, *105*, 8475−8491.

(3) Schwartz, B. J. *Annu. Rev. Phys. Chem.* **2003**, *54*, 141−172.

(4) Sheats, J. R. *J. Mater. Res.* **2004**, *19*, 1974−1989.

(5) Choi, Y.; Zachary, A.; Tepavcevic, S.; Wu, C. P.; Hanley, L. *Int. J. Mass Spectrom.* **2005**, *241*, 139−147.

(6) Choi, Y. S.; Tepavcevic, S.; Xu, Z.; Hanley, L. *Chem. Mater.* **2004**, *16*, 1924−1931.

(7) Tepavcevic, S.; Choi, Y.; Hanley, L. *J. Am. Chem. Soc.* **2003**, *125*, 2396−2397.

(8) Tepavcevic, S.; Choi, Y.; Hanley, L. *Langmuir* **2004**, *20*, 8754−8761.

(9) Tepavcevic, S.; Wroble, A. T.; Bissen, M.; Wallace, D. J.; Choi, Y.; Hanley, L. *J. Phys. Chem. B* **2005**, *109*, 7134−7140.

(10) Tepavcevic, S.; Zachary, A. M.; Wroble, A. T.; Choi, Y.; Hanley, L. *J. Phys. Chem. A* **2006**, *110*, 1618−1624.

(11) Hanley, L.; Choi, Y.; Tepavcevic, S. **2004**, *804*, JJ5.3.1−JJ5.3.6.

(12) Jang, I.; Ni, B.; Sinnott, S. B. *J. Vac. Sci. Technol., A* **2002**, *20*, 564−568.

(13) Bertrand, P.; Delcorte, A.; Garrison, B. J. *Appl. Surf. Sci.* **2003**, *203*, 160−165.

(14) Garrison, B. J.; Kodali, P. B. S.; Srivastava, D. *Chem. Rev.* **1996**, *96*, 1327−1341.

(15) Hanley, L.; Sinnott, S. B. *Surf. Sci.* **2002**, *500*, 500−522.

(16) Lim, H.; Schultz, D. G.; Gislason, E. A.; Hanley, L. *J. Phys. Chem. B* **1998**, *102*, 4573−4580.

(17) Milman, V.; Winkler, B.; White, J. A.; Pickard, C. J.; Payne, M. C.; Akhmatskaya, E. V.; Nobes, R. H. *Int. J. Quantum Chem.* **2000**, *77*, 895−910.

(18) Payne, M. C.; Teter, M. P.; Allan, D. C.; Arias, T. A.; Joannopoulos, J. D. *Rev. Mod. Phys.* **1992**, *64*, 1045−1097.

(19) Wijesundara, M. B. J.; Ji, Y.; Ni, B.; Sinnott, S. B.; Hanley, L. *J. Appl. Phys.* **2000**, *88*, 5004−5016.

(20) Janssen, R. A. J.; Smilowitz, L.; Sariciftci, N. S.; Moses, D. *J. Chem. Phys.* **1994**, *101*, 1787−1798.

(21) Zheng, Z.; Xu, X. D.; Fan, X. L.; Lau, W. M.; Kwok, R. W. M. *J. Am. Chem. Soc.* **2004**, *126*, 12336−12342.

(22) Hanley, L.; Lim, H. J.; Schultz, D. G.; Wainhaus, S. B.; de Sainte Claire, P.; Hase, W. L. *Nucl. Instrum. Methods Phys. Res., Sect. B* **1997**, *125*, 218−222.